A quantitative model for differential motility of gliomas in grey and white matter

K. R. Swanson*[†‡], E. C. Alvord Jr*[‡], and J. D. Murray[†]

*Departments of *Pathology and [†]Applied Mathematics, University of Washington and [‡]Laboratory of Neuropathology, Harborview Medical Center, Seattle, WA, USA*

Abstract. We have extended a mathematical model of gliomas based on proliferation and diffusion rates to incorporate the effects of augmented cell motility in white matter as compared to grey matter. Using a detailed mapping of the white and grey matter in the brain developed for a MRI simulator, we have been able to simulate model tumours on an anatomically accurate brain domain. Our simulations show good agreement with clinically observed tumour geometries and suggest paths of submicroscopic tumour invasion not detectable on CT or MRI images. We expect this model to give insight into microscopic and submicroscopic invasion of the human brain by glioma cells. This method gives insight in microscopic and submicroscopic invasion of the human brain by glioma cells. Additionally, the model can be useful in defining expected pathways of invasion by glioma cells and thereby identify regions of the brain on which to focus treatments.

INTRODUCTION

Gliomas generally are diffuse and invasive intracranial neoplasms accounting for about one half of all primary brain tumours. The advent of increased detection capabilities in computerized tomography (CT) and magnetic resonance imaging (MRI) during the last two decades has not only brought about earlier detection of gliomas but has also provided increased definition of the geometric patterns of gliomas. Despite this progress, the benefits of early treatment have been difficult to define (Alvord & Shaw 1991; Kelley & Hunt 1994; Tracqui *et al.* 1995; Woodward *et al.* 1996; Burgess *et al.* 1997; Silbergeld & Chicoine 1997). For instance, even upon extensive surgical excision well beyond the grossly visible tumour boundary, recurrence near the edge of resection ultimately results (Kelley & Hunt 1994; Silbergeld & Chicoine 1997). A great deal of experimental and some theoretical research has been applied to understanding why gliomas are so difficult to treat.

Unlike most other tumours, gliomas are generally highly diffuse. In fact, experimental results indicate that within 7 days of tumour implantation in a rat brain, glioma cells can be identified throughout the central nervous system (CNS) (Silbergeld & Chicoine 1997). A locally dense tumour growth remains where the cancerous tissue was initially implanted but

Correspondence: Kristin R. Swanson, Department of Pathology, Laboratory of Neuropathology, 325 Ninth Avenue, Box 359791, Harborview Medical Center, Seattle, WA 980104-2499, USA. E-mail: swanson@amath.washington.edu

there are solitary tumour cells throughout the CNS (Chicoine & Silbergeld 1995; Silbergeld & Chicoine 1997). This indicates a potential failing point of treatment: most glioma treatments are directed locally to the bulk mass when, in fact, the action of the tumour growth and invasion is elsewhere.

Mathematical modelling has been used as a theoretical framework to describe the invasive nature of gliomas (Cook *et al.* 1995; Tracqui *et al.* 1995; Woodward *et al.* 1996; Burgess *et al.* 1997) by isolating two characteristics: proliferation and diffusion (invasion). Diffusion was considered to represent the active motility of glioma cells, which previous model results have shown to be more important in determining survival than the proliferative rate of the tumour (Burgess *et al.* 1997). Since malignant glioma cells implanted in the brain of rats disperse more quickly along white matter tracts (Kelley & Hunt 1994; Chicoine & Silbergeld 1995; Silbergeld & Chicoine 1997), we wished to include different diffusion rates of glioma cells in grey and white matter to create a more realistic model (Swanson, 1999).

In this article, we use a mathematical model to represent the growth and invasion of a glioma in different parts of the human CNS. The model we present incorporates the effects of heterogeneous brain tissue on the diffusion and growth rates of glioma cells in an attempt to emulate the clinically and experimentally observed asymmetries of the apparent tumour boundaries. In particular, we discuss the implications of the increased invasive abilities in white matter over grey matter. Due to the heterogeneous structure of the brain tissue, we will suggest how the location of the bulk tumour can affect the geometry of the tumourous invasion.

METHODS

The mathematical model

Cruywagen *et al.* (1995), Tracqui *et al.* (1995), Woodward *et al.* (1996) and Burgess *et al.* (1997) developed a mathematical model of glioma growth and diffusion based on the analysis of serial CT scans taken in the terminal year of a patient with recurrent anaplastic astrocytoma. The model defined the evolution of the glioma cell population solely by proliferation and diffusion. That is, the model expressed as a word equation is:

Rate of change of tumour cell density = Diffusion (motility) of tumour cells + Growth of tumour cells.

If we let c(x, *t*) be the number of cells at any position *x* and time *t*, the word equation can be written mathematically as a reaction-diffusion equation (equation 1):

$$\frac{dc}{dt} = \nabla \cdot (D \nabla c) + \rho c, \tag{1}$$

where ρ (1/day) represents the net rate of growth of cells including proliferation and death (or loss), D (cm^2/day) is the diffusion coefficient of cells in brain tissue and ∇ represents the spatial gradient. The diffusion term describes the active migration of the glioma cells using a simple Fickian diffusion (Murray 1993) where cells move from regions of higher to lower densities. Tumour cells are assumed to grow exponentially. Logistic growth (implying formation of a necrotic core as the tumour outgrows its blood supply) would be strictly more accurate but the differences in calculated survival time are so slight as to be negligible (Cruywagen *et al.* 1995; Tracqui *et al.* 1995; Woodward *et al.* 1996; Burgess *et al.* 1997) on the time scale concerned.

The previous mathematical models (Burgess *et al.* 1997; Cruywagen *et al.* 1995; Tracqui *et al.* 1995; Woodward *et al.* 1996) considered gross estimates of the boundaries of the cortical

and ventricular surfaces of the brain but did not take into account the spatial heterogeneity of the brain tissue with respect to grey and white matter of gyri and deep nuclei. The recent availability of the BrainWeb database (HTTP://www.bic.mni.mcgill.ca/brainweb) (Kwan, Evans & Pike 1996; Cocosco *et al.* 1997; Collins *et al.* 1998) allowed us to define accurately the locations and proportions of grey and white matter to a much greater resolution than available even in neuro-anatomy texts. This database was created by Collins *et al.* (1998) for a MRI simulator and defines the three-dimensional locations and proportions of grey and white matter at a resolution of 1 mm^3 throughout the brain. In a 3D coordinate system every voxel is associated with numbers representing the proportion of grey and white matter in that 1 mm^3 of tissue. In theory, we could have used graphical anatomy maps to extrapolate grey and white matter locations throughout the brain but the 3D atlas, provided by the BrainWeb database, gave us a greater resolution.

To account for spatial heterogeneity of the brain tissue, we make the diffusion coefficient D a function of the spatial variable x differentiating regions of grey and white matter. The present model is then written mathematically as:

$$\frac{dc}{dt} = \nabla \cdot (D(x) \nabla c) + \rho c. \tag{2}$$

Specifically, we take $D(x) = D_g$, a constant, for x in grey matter and $D(x) = D_w$, another constant, for x in white matter, where $D_w > D_g$.

It is still necessary to assume that tumour growth occurs in two phases (Burgess *et al.* 1997; Cruywagen *et al.* 1995; Tracqui *et al.* 1995; Woodward *et al.* 1996). In the first phase the tumour cells only proliferate to form a small dense lesion and only at some later time do the tumour cells become diffusive. It is not until the second phase that equation 2 applies. Without this assumption, the model simulates the case of gliomatosis cerebri: tumour cells can be found throughout the brain but no single bulk tumour is identifiable.

Parameter estimation

Parameter estimates in any realistic mathematical model are crucial. Doubling times for gliomas have been estimated at 1 week to 12 months (Alvord & Shaw 1991) covering the range of high to low grade gliomas. To represent cell proliferation of a high-grade astrocytoma, we take a growth rate of $\rho = 0.012$/day corresponding to a doubling time of 2 months. High-grade astrocytomas account for ~50% of all astrocytomas, which in turn make up ~50% of all primary brain tumours (Alvord & Shaw 1991).

Little is known about diffusion or motility rates of gliomas cells. Normal glial cells have a very low motility rate (Silbergeld & Chicoine 1997) as compared to glioma cells which exhibit abnormally high motility rates (Chicoine & Silbergeld 1995). *In vitro* studies by Westermark, Magnusson & Heldin (1982) demonstrated the remarkable motility of human malignant glioma cells. Chicoine & Silbergeld (1995) and Silbergeld & Chicoine (1997) have quantified brain tumour cell motility and invasion capabilities *in vivo* and *in vitro*. Their results (Chicoine & Silbergeld 1995) suggest an average linear velocity of 12.5 mm/h for rat glioma cells *in vitro* and a minimum linear velocity of 4.8 mm/h for rat glioma cells *in vivo*. Since glioma cells do not travel a linear path, we model glioma motility as a random walk diffusion.

Information regarding human glioma tumour growth and infiltration comes from CT and MRI images. Associated with each of these imaging techniques is a threshold of detection. Above this threshold the tumour is observable while below the threshold it is not. Now since gliomas are diffuse tumours, presently available imaging techniques only 'detect' a small portion of the actual tumour. Only those regions of the tumour that exceed the threshold of

detection appear on the image. Indeed, Silbergeld & Chicoine (1995, 1997) cultured tumour cells from histologically normal brain 4 cm from the grossly apparent bulk tumour location. That portion of the tumour that is observable by the medical imaging technique we term the detectable tumour and the apparent border the threshold, which is different for CT, MRI, gross and microscopic analyes (Concannon, Kramer & Berry 1960; Kelley & Hunt 1994).

Multiple CT or MRI scans can be used to calculate the rate of advance of the detectable tumour margin. To relate linear velocity v of the detectable tumour margin with the proliferation rate ρ and a random walk diffusion coefficient D, we use Fisher's approximation (Murray 1993; Burgess *et al.* 1997), $D \approx v^2/4\rho$. This approximation comes from the observation that a population governed by growth and diffusion alone expands at a rate of $2\sqrt{\rho D}$ for large time. For the model we consider, we are most interested in the variation in parameter values in white and grey matter regions. We associate the diffusion coefficients:

$$D_g = v^2_g/4\rho \text{ and } D_w = v^2/4\rho$$

with the experimentally observed linear velocities v_g and v_w in white and grey matter, respectively. The serial CT scans (Tracqui *et al.* 1995) used in the development of the original mathematical model (Cruywagen *et al.* 1995; Tracqui *et al.* 1995; Woodward *et al.* 1996; Burgess *et al.* 1997) were reexamined to define the rate of advance of the tumour margin (v_g, v_w). Within the right hemisphere the margin of detectable tumour moved at about 1.5 cm in 180 days (Tracqui *et al.* 1995; Woodward *et al.* 1996), giving an average speed of $v = 0.008$ cm/day. For the growth rate $\rho = 0.012$/day, the Fisher approximation then suggests the average diffusion coefficient $D = v^2/4\rho = 0.0013$ cm^2/day. Due to the proximity of this invasion front to the deep cerebral nuclei (predominantly grey matter within the right hemisphere), we associate this value with grey matter diffusion: v_g at 0.008 cm/day (Tracqui *et al.* 1995) and D_g at 0.0013 cm^2/day. From the CT scans, the speed of advance of the tumour margin across the corpus callosum (white matter) is two to three times as fast as that in (predominately) grey matter; thus, we estimate $v_w > 2.2 \, v_g$ at 0.018 cm/day and $D_w > 5 \, D_g$ at 0.0065 cm^2/day. Throughout our simulations we use a five-fold difference in the diffusion coefficients in grey and white matter: $D_w = 5 \, D_g$.

Another means of assessing the diffusion coefficient is to use the mean-square distance (in two dimensions) of the cells from the origin (equation 3),

$$<r^2> = 4 D t. \tag{3}$$

Since growth is not included in this definition, the value of D calculated from this formula using information regarding the progression of the tumour profile (e.g. on CT scans) would be an overestimate of the actual diffusion coefficient. This formula would be most appropriate if data were available for tracking individual cells in grey and white matter separately but such data are not yet available. Since data regarding a specific glioma comes from CT or MRI scans where proliferation and diffusion are both represented, we expect the Fisher estimate to be a better approximation for the glioma diffusion coefficients.

For our simulations, we follow Woodward *et al.* (1996) in allowing a 10-fold variation in ρ and D to simulate multiple tumour grades: high-grade (high ρ and high D), intermediate grade (high ρ and low D or low ρ and high D), and low grade (low ρ and low D).

Threshold of detection of gliomas at diagnosis and death

Only a portion of the total tumour is detectable by any presently available medical imaging technique. In the original model (Tracqui *et al.* 1995), comparison of CT images with post mortem microscopic analysis of brain slices suggested a 40 000 cells/cm^2 threshold of
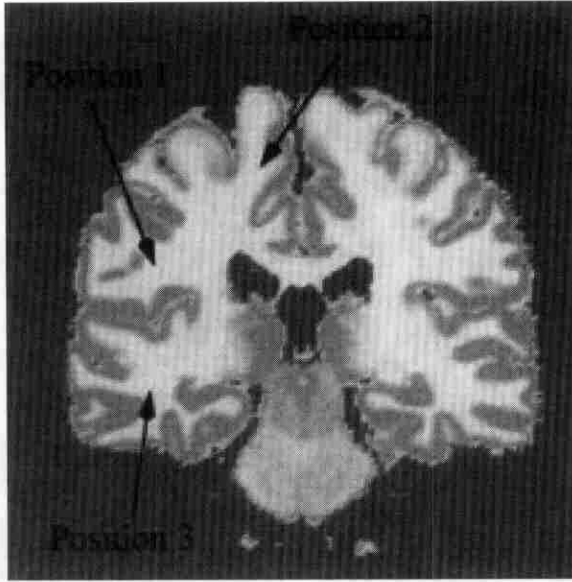
Figure 1. Computational domain with tumour locations. Grey matter appears grey and white matter appears white. Position 1 is the location of an inferior fronto-parietal tumour, position 2 is the location for a superior fronto-parietal tumour, position 3 is the location for a temporal lobe tumour.

detection for enhanced CT scans. For a histopathologist, this threshold would correspond to about 400 cells in the approximately 1 mm^2 field covered by a 10× objective or about 25 cells covered by a 40× objective. Although the sizes of gliomas at diagnosis (Blankenberg *et al.* 1995) and death (Concannon *et al.* 1960) vary greatly, the model considered the mean tumour radius at detection on CT to be 1.5 cm and at death 3.0 cm (Cook *et al.* 1995; Tracqui *et al.* 1995; Woodward *et al.* 1996; Burgess *et al.* 1997). We retain these sizes and thresholds and, in addition, consider an as-yet-unavailable medical imaging technique that has an 80-fold more sensitive threshold of detection. Thus, our theoretically advanced imaging technique has a threshold of detection of 500 cells/cm^2. For a histopathologist this threshold would correspond to about five cells in the field covered by a 10× objective or about one cell in every three fields covered by a 40× objective.

RESULTS

Figure 1 defines a typical coronal section of the brain as the computational domain on which to begin our model simulations. Although the BrainWeb anatomical atlas is available in three-dimensions, we demonstrate the model abilities on this arbitrarily chosen coronal section. In the figure, white and grey matters appear white and grey, respectively. The three tumour sites we consider are labelled as shown: position 1 represents an inferior fronto-parietal tumour, position 2 corresponds to a superior fronto-parietal tumour and position 3 defines a temporal lobe tumour. At each of these locations we will consider the four tumour grades representing 10-fold variations in the growth rate ρ and the diffusion coefficient D: high grade (high ρ, high D), ontermediate grade (high ρ, low D or low ρ, high D) and low grade (low ρ, low D) with abbreviations HH, HL, LH and LL, respectively. The first letter of the abbreviations refers to a high (H) or low (L) growth rate ρ while the second letter refers
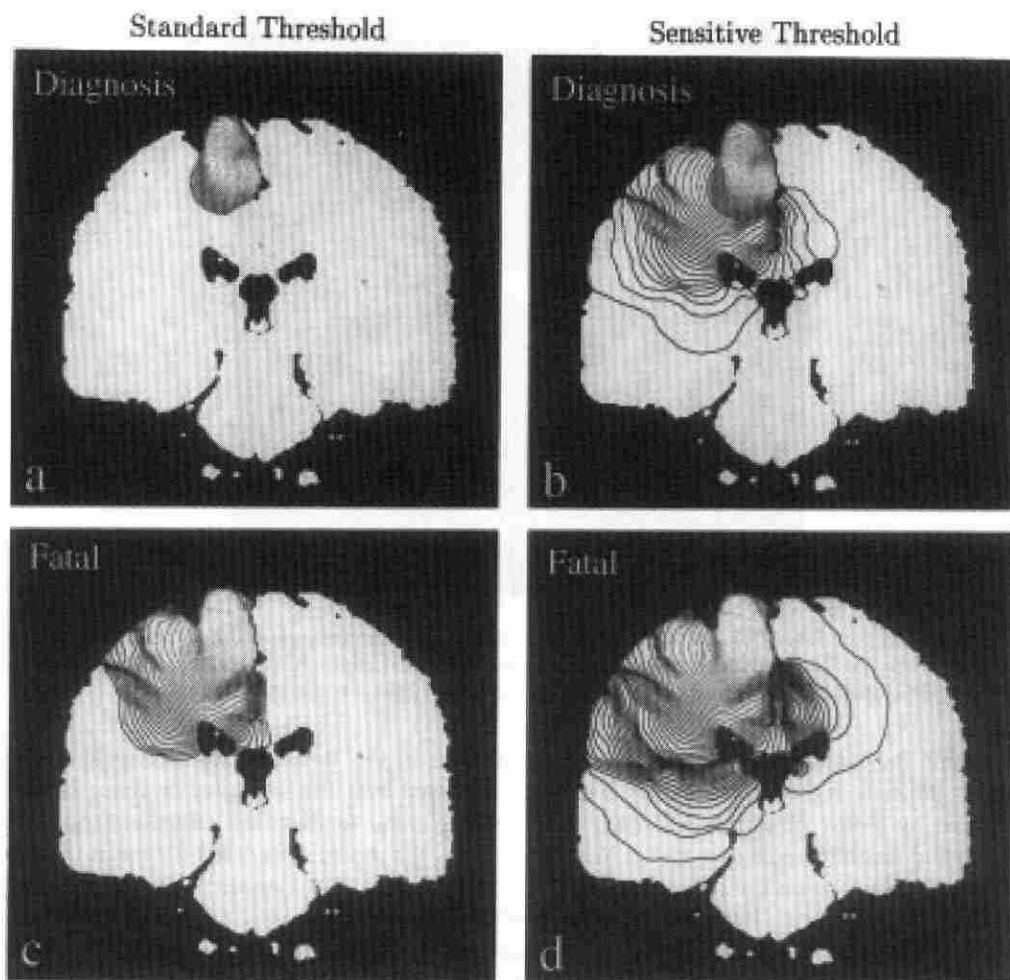
Figure 2. Simulation of tumour invasion of a high-grade glioma in position 2 in the superior cerebral hemisphere: (a) (b) at diagnosis; (c) (d) at death; (a) (c) as seen by our standard threshold of detection; (b) (d) as calculated out to 1.25% of the threshold (boundary) cell concentration defining the sensitive threshold of detection.

to a high (H) or low (L) diffusion coefficient D. We will also consider two different model imaging techniques: one corresponding to the original CT scan threshold (our 'standard threshold') and the other representing a theoretical imaging technique with a threshold of detection 80 times more sensitive (as discussed above).

Invasion dynamics as a function of tumour location

Since the present model takes into account the heterogeneity of the brain tissue and the complexity of the anatomic geometry (apparent in Figure 1), the dynamics of invasion can be quite varied depending on the initial location of the tumour. Figures 2–4 represents simulations of high-grade (high ρ, high D) tumours in position 2, 1 and 3 (as defined in Figure 1), respectively.

Figure 2a represents the portion of a position 2 (superior fronto-parietal) high-grade tumour detectable with our standard threshold at diagnosis, when the detectable tumour

(the portion of the tumour with density above the threshold of detection of 40 000 cells/cm^2) covers an area equivalent to a circle with diameter 3 cm. Although the tumour looks fairly localized, by increasing our detection abilities by a factor of 80 (corresponding to a threshold of detection of 500 cells/cm^2), we see in Figure 2c that at the time of diagnosis the tumour has invaded quite extensively throughout the right cerebral hemisphere and across the corpus callosum to the contralateral hemisphere. Figure 2b represents the portion of the tumour detectable with our standard threshold about 140 days later at the time of death, when the detectable tumour (the portion of tumour with density above the threshold of detection of 40 000 cells/cm^2) covers an area equivalent to a circle of diameter 6 cm. By increasing detection abilities to correspond to a resolution of 500 tumour cells/cm^2), Figure 2d demonstrates the invasion not apparent by CT, MRI or gross examination post mortem. Note that (Figure 2b, d) do not represent the full extent of tumour invasion but rather an increase in detection ability associated with a theoretically more sensitive imaging technique, still well above the single cell threshold of detection.

Similarly, Figure 3 shows a high-grade inferior fronto-parietal (position 1) glioma at detection and death (as defined above). Although the tumour appears fairly localized by our standard threshold, the model suggests that the tumour has already invaded superiorly and inferiorly (into the temporal lobe). Approximately 110 days elapses between detection (Figure 3a, b) and death (Figure 3c, d) for this untreated glioma. At the lethal size, the standard threshold defines a still fairly localized tumour; however, the microscopic invasion of the tumour has proceeded across the corpus callosum.

Figure 4 shows a high-grade temporal lobe (position 3) tumour. The tumour growth appears at detection (Figure 4a, b) to be hindered superiorly. This delays the growth of the detectable tumour to a lethal size (Figure 4c, d) for 170 days.

How much tumour is really detected above the threshold of detection?

The proportion of tumour detectable by medical imaging decreases not only with increasing diffusion coefficient but also with decreasing growth rate, as shown in Figure 5 for position 1 tumours. For a fixed growth rate, as diffusion increases, tumour cells migrate longer distances and therefore smear out the distribution of glioma cells. For a fixed diffusion coefficient, as the growth rate decreases, tumour cells have less of a chance to build up to detectable levels. Indeed, it is the ratio of the growth rate to the diffusion coefficient, ρ/D, that determines the proportion of tumour that is detectable. The raio ρ/D occurs naturally in the appropriate nondimensional form of the model. Such a process usually highlights relevant parameter groupings with experimental implications. The recognition of this type of relationship is all the more important since at the moment there are no techniques for independent estimates for the diffusion and growth rate parameters *in vivo*).

To explore the observation that the ratio ρ/D determines the proporation of tumour that is dtectable, Figure 6 shows the precentage of tumour detectable at diagnosis using our standard threshold of detection as a function of the ratio. For ρ/D large, the tumour is dominated by proliferation and the majority of the tumour is detectable. For ρ/D small, the tumour is dominated by diffuse and only a small portion of the tumour is detectable. Nore that there is a slight variability in the amount detectable depending on the tumour location.

In our model, we have so far compared two levels of sensitivity of detection of tumour cells, the original based on an actual case studied by enhanced CT and a theoretical one 80
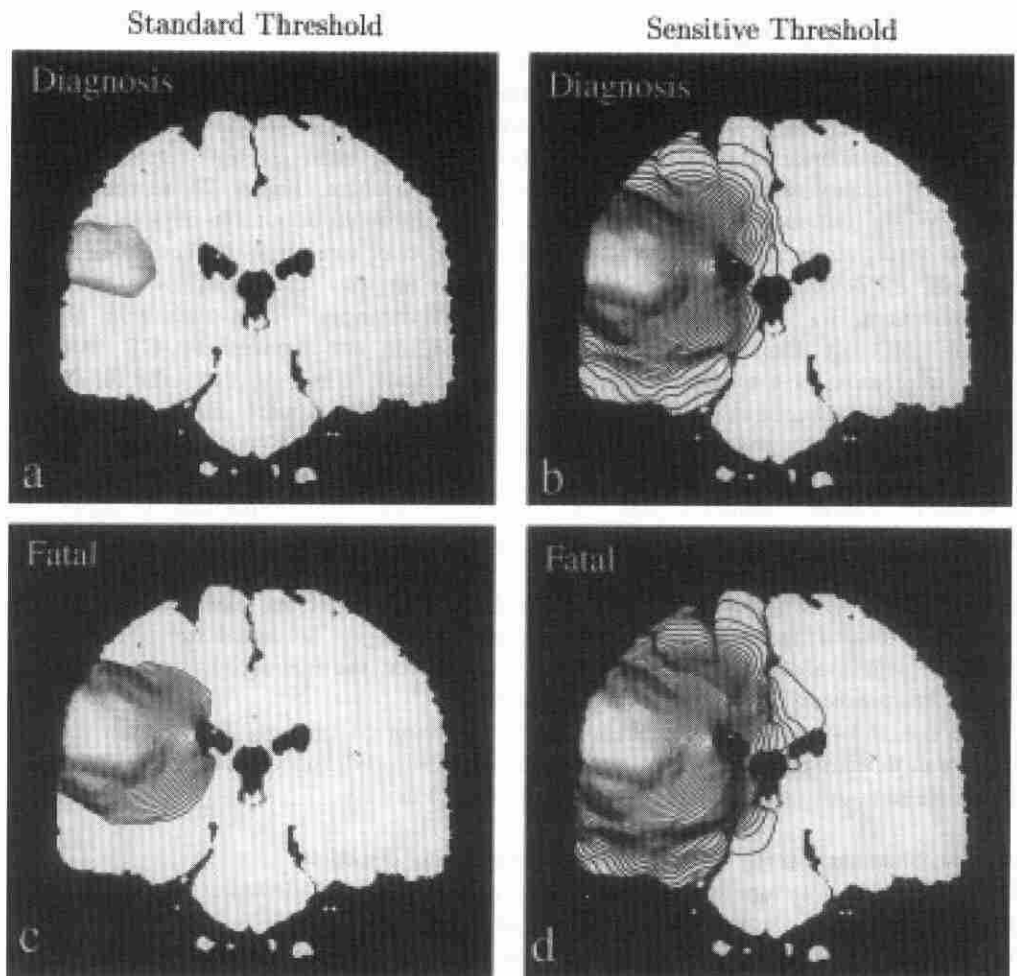
Figure 3. Simulation of tumour invasion of a high-grade glioma in position 1 in the inferior cerebral hemisphere: (a) (b) at diagnosis; (c) (d) at death; (a) (c) as seen by our standard threshold of detection; (b) (d) as calculated out to 1.25% of the threshold (boundary) cell concentration defining the sensitive threshold of detection.

times more sensitive. The threshold for the former was estimated to be 40 000 cells/cm^2 and for the latter arbitrarily reduced to 500 cells/cm^2. As Figure 7 shows, any other definition of the threshold is theoretically possible, but one should be aware that the percent of tumour detectable varies both with the grade and the site of the tumour. The high grade (HH) and low grade (LL) extremes are detected identically and almost linearly over the whole range of thresholds, but obviously on different time scales. The intermediate grade, highly proliferative (HL) gliomas are almost entirely detectable regardless of the threshold because their diffusion is so low compared to their growth rate. By contrast, the intermediate grade, highly infiltrative (LH) gliomas are not only more difficult to detect (because of their great diffusion) but also more irregular in relation to site: note the sudden decrease in detectability of position 1 tumours as the threshold increases and approaches 40 000 cells/cm^2. However, as the threshold decreases, the variability decreases and the difference from the ideal 100% detectability decreases.

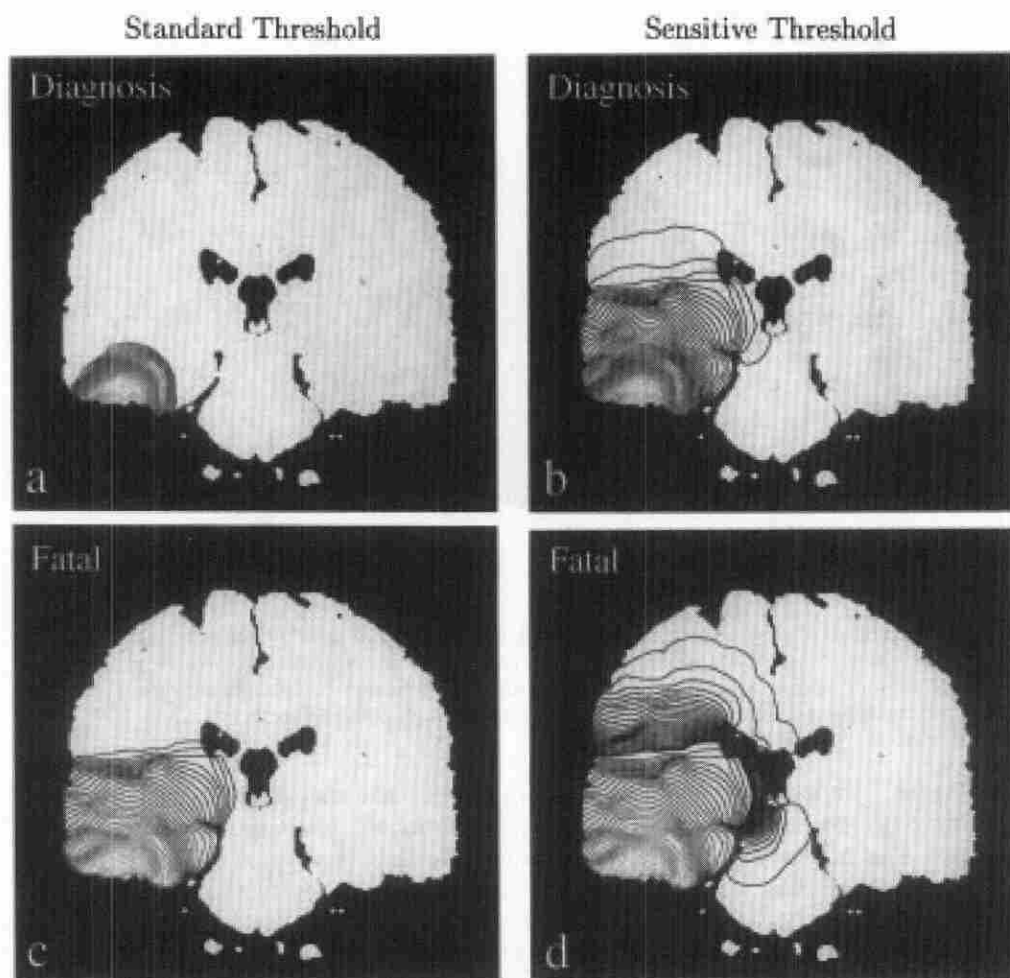Standard Threshold   Sensitive Threshold

Figure 4. Simulation of tumour invasion of a high-grade glioma in position 3 in the temporal lobe: (a) (b) at diagnosis; (c) (d) at death; (a) (c) as seen by our standard threshold of detection; (b) (d) as calculated out to 1.25% of the threshold (boundary) cell concentration defining the sensitive threshold of detection.)

DISCUSSION

One of several advantages of mathematical modelling is the ability to alter theoretically a parameter and analyse its effect. By mathematically decreasing the threshold of detection in our model, we can visualize the usefulness of increasing detection capabilities in medical imaging. Figure 7 illustrates the effect of decreasing the threshold of detection on the proportion of the tumour that can be detected by the new hypothetical technique. Augmented detection abilities invariably increase the amount of tumour identifiable but the rate of increase varies among tumour positions and grade. Note that detection of high-grade and low-grade tumours coincide, although the duration of survival involved differs 10-fold. This suggests that the ratio between the growth rate ρ and the diffusion coefficient D is critical to the determination of the proportion the tumour detectable. Additionally, this suggests that the invasive nature of the tumour is defined by the same ratio ρ/D.
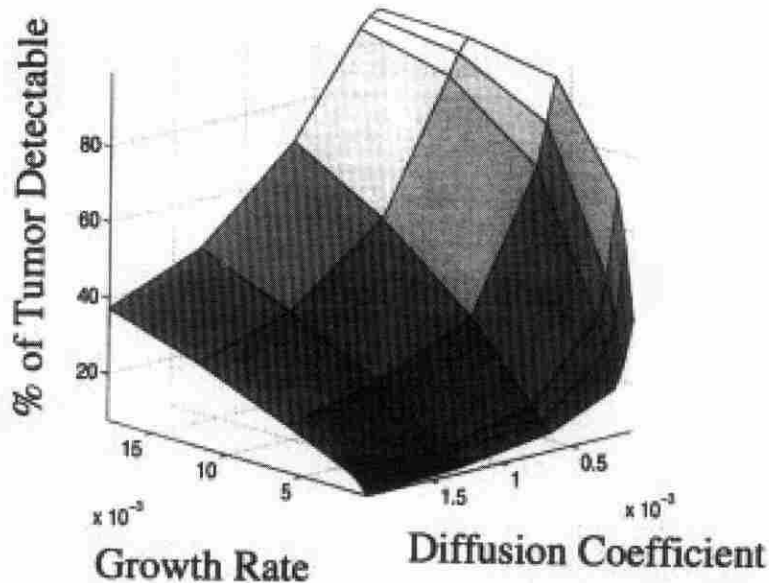
Figure 5. Percentage of position 1 tumour detectable by our standard threshold of detection at diagnosis *vs.* the growth rate ρ and the diffusion coefficient in grey matter D_g. Note that the greatest proportion of detectable tumour occurs with high growth rate and low diffusion coefficient; conversely, the least proportion is seen with gliomas having low growth rate and high diffusion coefficient.

In Figure 7 we also observe that the slowly growing and quickly diffusing intermediate grade tumours are associated with the least proportion of tumour that is detectable at diagnosis. This is clearly due to the extensive invasive abilities of those tumours. High and low grade tumours are associated with the same proportion of tumour detectable as a function of the threshold of detection. The difference between the high and low-grade tumours is the time scale on which the growth and invasion occurs. It takes high-grade tumours a very short time to invade. Low-grade tumours may follow the invasion path of high-grade tumours but much more slowly.

In our new model, the diffusion coefficient is estimated as being approximately five times larger in white matter than in grey matter. There is probably some anisotropy (directed motion) to the diffusion along individual white matter fibres but the network of these fibers is very complicated on the scale of the whole brain. Three major paths of invasion can be identified: laterally through the corpus callosum, vertically through the internal and external capsules, and antero-posteriorly through the uncinate (fronto-temporal) and fronto-occipital tracts. We have assumed that a change in the diffusion coefficient in white matter may be sufficient to simulate the increased motility of gliomas in white matter.

Although brain boundaries and tissue heterogeneity have been taken into account in our model, we do not yet define any degree of destruction or degeneration of the normal tissue by the invading tumour cells. Just how much tumour invasion is necessary to produce deformation and/or necrosis is not known, but could be very important in defining the times from diagnosis to death. This issue may be especially important in particular situations where certain 'eloquent' regions of the brain are invaded by tumour cells, even at very low densities. Clearly, more accurate localization of cortical and subcortical structures associated with major clinical syndromes is needed in the three-dimensional simulations possible in the
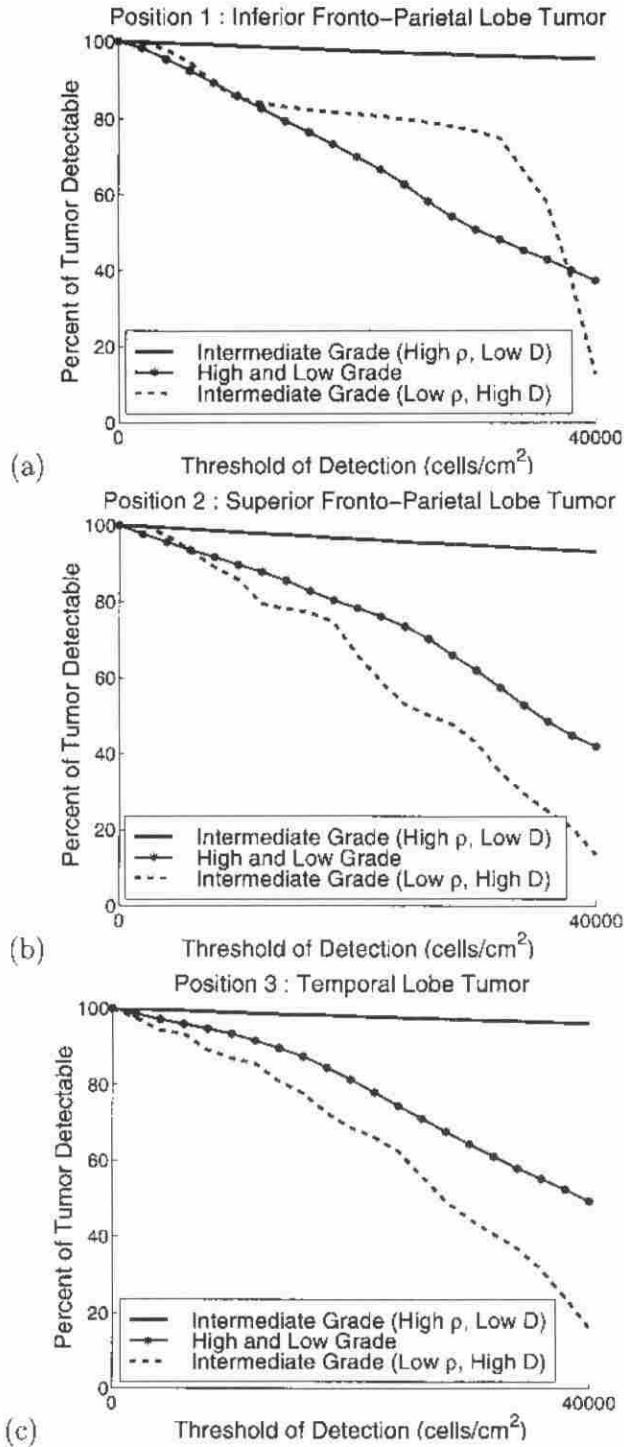
Figure 6. Percentage of detectable volume of tumour *vs.* the threshold of detection at various positions. The 40 000 cells/cm² represents our standard, the threshold of detection for an enhanced CT scan.

model. Additionally, we neglect considerations of oedema, age and neurological status, which are important in determining the time to diagnosis and death.

Our present simulations are in two dimensions and could be presented in horizantal (axial) or sagittal planes as well as the coronal one arbitrarily shown. It is true that since the BrainWeb database is available in all three planes, three-dimensional modelling would be more desirable but our present two-dimensional simulations are more tractable to visualize as well as to calculate. A three-dimensional version of the model would be more accurate and is planned, as are results of various extents of surgical resection and radiotherapeutic boundaries. The possibility of incorporating the effects of oedema and necrosis are also being considered.

Despite the assumptions involved in the model formulation, we have obtained many clinically potentially useful results. In particular, the model has the ability to suggest paths of invasion unseen by standard medical imaging techniques. Knowledge of these invasion paths can be very useful in defining the best treatment scenario for a given patient.

CONCLUSIONS

We have presented a mathematical model for glioma growth and invasion that allows heterogeneities in brain tissue to account for asymmetric nonspherical tumour geometries implicit in previous models. Our model is intended to give an understanding of the spatio-temporal invasion of glioma tumours. The model suggests paths of tumour invasion not detectable by present medical imaging technology. Knowledge of this unseen invasion may be helpful in defining appropriate regions of the brain on which to focus treatment.

With the availability of a detailed description of the local composition of grey and white matter throughout the brain, the model can be easily extended to specific patients and the pattern at the time of diagnosis extrapolated temporally in either direction with the hope of suggesting appropriate treatment locations and scenarios.

ACKNOWLEDGEMENTS

REFERENCES

ALVORD EC JR, SHAW CM (1991) Neoplasms affecting the nervous system in the elderly. In: DUCKETT S. ed. *The Pathology of the Aging Human Nervous System*, pp. 210–281. Philadelphia: Lea & Febiger.

BLANKENBERG FG, TEPLITZ RL, ELLIS W *et al.* (1995) The influence of volume tric tumour doubling time, DNA ploidy, and histologic grade on the survival of patients with intrcranial astrocytomas. *Am. J. Neuro Rad* **16**, 1001–1012.

BURGESS PK, KULESA PM, MURRAY JD, ALVORD EC Jr (1997) The interaction of growth rates and diffusion coefficients in a three-dimensional mathematical model of gliomas. *J. Neuropath Exp Neuro* **56**, 704–713.

CHICOINE MR, SILBERGELD DL (1995) Assessment of brain tumour cell motility in vivo and in vitro. *J. Neurosurg* **82**, 615–622.

Cocosco CA, Kollokian V, Kwan RK-S, Evans AC (1997) Brainweb: Online interface to a 3D MRI simulated brain database. *Neuroimage* **5**, S425.

Collins DL, Zijdenbos AP, Kollokian V *et al.* (1998) Design and construction of a realistic digital brain phantom. *IEEE Transactions Med. Imaging* **17**, 463–468.

Concannon JC, Kramer S, Berry R (1960) The extent of intrcranial gliomata at autopsy and its relation to techniques in radiation therapy of brain tumours. *Am. J. Roentgenol. Radium Ther Nucl Med.* **84**, 99–107.

Cook J, Woodward DE, Tracqui P, Murray JD, Alvord EC Jr (1995) Resection of gliomas and life expectancy. *J. Neuro-Oncol.* **24**, 131.

Cruywagen GC, Woodward DE, Tracqui P, Bartoo GT, Murray JD, Alvord EC, Jr (1995) The modeling of diffusive tumours. *J. Biol. Sys* **3**, 937–945.

Kelley PJ, Hunt C (1994) The limited value of cytoreductive surgery in elderly patients with malignant gliomas. *Neurosurg* **34**, 62–67.

Kwan R, Evans AC, Pike GB (1996) An extensible MRI simulator for post-processing evaluation. In: *Proceedings of the 4th International Conference on Visualization in Biomedical Computing* **96**, 135–140.

Murray JD (1993) *Mathematical Biology.* Heidelburg: Springer-Verlag.

Silbergeld DL, Chicoine MR (1997) Isolation and characterization of human malignant glioma cells from histologically normal brain. *J. Neurosurg* **86**, 525–531.

Swanson KR (1999) Mathematical modeling of the growth and control of tumors. Ph.D thesis. University of Washington.

Tracqui P, Cruywagen GC, Woodward DE, Bartoo GT, Murray JD, Alvord Jr EC (1995) A mathematical model of glioma growth: the effect of chemotherapy on spatio-temporal growth. *Cell Prolif* **28**, 17–31.

Westermark R, Magnusson A, Heldin CH (1982) Effect of epidermal growth factors on membrane motility and cell locomotion in cultures of human clonal glioma cells. *J. Neurosci Research* **8**, 491–507.

Woodward DE, Cook J, Tracqui P, Cruywagen GC, Murray JD, Alvord Jr EC (1996) A mathematical model of glioma growth: the effect of extent of surgical resection. *Cell Prolif* **29**, 269–288.